RNAi targeting multiple cell adhesion molecules reduces immune cell recruitment and vascular inflammation after myocardial infarction

Citation: Sager, H. B. et al. "RNAi Targeting Multiple Cell Adhesion Molecules Reduces Immune Cell Recruitment and Vascular Inflammation after Myocardial Infarction." Science Translational Medicine 8.342 (2016): 342ra80-342ra80.

As Published: http://dx.doi.org/10.1126/scitranslmed.aaf1435

Publisher: American Association for the Advancement of Science (AAAS)

Persistent URL: http://hdl.handle.net/1721.1/106928

Version: Author's final manuscript: final author's manuscript post peer review, without publisher's formatting or copy editing

HHS Public Access

Author manuscript

Sci Transl Med. Author manuscript; available in PMC 2016 November 28.

Published in final edited form as:

Sci Transl Med. 2016 June 8; 8(342): 342ra80. doi:10.1126/scitranslmed.aaf1435.

RNAi targeting multiple cell adhesion molecules reduces immune cell recruitment and vascular inflammation after myocardial infarction

Hendrik B. Sager[#1,*], **Partha Dutta**[#1], **James E. Dahlman**[#2,3,4], **Maarten Hulsmans**[1], **Gabriel Courties**[1], **Yuan Sun**[1], **Timo Heidt**[1], **Claudio Vinegoni**[1], **Anna Borodovsky**[5], **Kevin Fitzgerald**[5], **Gregory R. Wojtkiewicz**[1], **Yoshiko Iwamoto**[1], **Benoit Tricot**[1], **Omar F. Khan**[3], **Kevin J. Kauffman**[3,6], **Yiping Xing**[2,3], **Taylor E. Shaw**[2,3], **Peter Libby**[7], **Robert Langer**[2,3,4,6], **Ralph Weissleder**[1,8], **Filip K. Swirski**[1], **Daniel G. Anderson**[#2,3,4,6], and **Matthias Nahrendorf**[#1,9,*]

[1]Center for Systems Biology, Massachusetts General Hospital and Harvard Medical School, Boston, MA 02114, USA.

[2]Harvard–Massachusetts Institute of Technology (MIT) Division of Health Sciences and Technology, Cambridge, MA 02139, USA.

[3]David H. Koch Institute for Integrative Cancer Research, MIT, Cambridge, MA 02139, USA.

[4]Institute for Medical Engineering and Science, MIT, Cambridge, MA 02139, USA.

[5]Alnylam Pharmaceuticals, Cambridge, MA 02142, USA.

[6]Department of Chemical Engineering, MIT, Cambridge, MA 02139, USA.

[7]Cardiovascular Division, Department of Medicine, Brigham and Women's Hospital, Boston, MA 02115, USA.

[8]Department of Systems Biology, Harvard Medical School, Boston, MA 02115, USA.

[9]Cardiovascular Research Center, Massachusetts General Hospital and Harvard Medical School, Boston, MA 02114, USA.

[#] These authors contributed equally to this work.

Abstract

[*]Corresponding author. mnahrendorf@mgh.harvard.edu (M.N.); hendrik.sager@tum.de (H.B.S.).

Author contributions: H.B.S., P.D., and J.E.D. designed and performed mouse experiments, flow cytometry, histology, qPCR, enzyme-linked immunosorbent assay, and particle and siRNA synthesis; collected and analyzed the data; and contributed to writing the article. M.H., G.C., Y.S., T.H., C.V., Y.I., O.F.K., K.J.K., Y.X., and T.E.S. performed mouse surgery, histology, and particle and siRNA synthesis. B.T. performed and analyzed cardiac MRI. G.R.W. performed and reconstructed FMT/CT and collected, analyzed, and discussed data. A.B., K.F., P.L., R.L., R.W., F.K.S., and D.G.A. conceived experiments and discussed strategy and results. M.N. designed and supervised the study and contributed to writing the article, which was edited and approved by all coauthors.

SUPPLEMENTARY MATERIALS

www.sciencetranslationalmedicine.org/cgi/content/full/8/342/342ra80/DC1

Competing interests: J.E.D., D.G.A., and R.L. have filed intellectual property protection related to 7C1 nanoparticles. The authors declare that they have no further competing interests.

Data and materials availability: Material transfer agreements may be required for nanoparticles.

Myocardial infarction (MI) leads to a systemic surge of vascular inflammation in mice and humans, resulting in secondary ischemic complications and high mortality. We show that, in *ApoE*$^{-/-}$ mice with coronary ligation, increased sympathetic tone up-regulates not only hematopoietic leukocyte production but also plaque endothelial expression of adhesion molecules. To counteract the resulting arterial leukocyte recruitment, we developed nanoparticle-based RNA interference (RNAi) that effectively silences five key adhesion molecules. Simultaneously encapsulating small interfering RNA (siRNA)–targeting intercellular cell adhesion molecules 1 and 2 (*Icam1* and *Icam2*), vascular cell adhesion molecule 1 (*Vcam1*), and E- and P-selectins (*Sele* and *Selp*) into polymeric endothelial-avid nanoparticles reduced post-MI neutrophil and monocyte recruitment into atherosclerotic lesions and decreased matrix-degrading plaque protease activity. Five-gene combination RNAi also curtailed leukocyte recruitment to ischemic myocardium. Therefore, targeted multigene silencing may prevent complications after acute MI.

INTRODUCTION

Leukocytes promote inflammation in atherosclerotic plaques (1–3). Systemically increased myeloid cell levels support disease progression and complication by delivering inflammatory mediators and tissue-destabilizing proteases to plaques. The current standard of care mostly modifies atherosclerosis risk factors and does not target myeloid cells. Although we will soon be able to identify inflamed plaques with imaging and other diagnostics, we currently lack the clinical means to rapidly and efficiently intervene therapeutically.

Macrophages turn over rapidly in growing arterial lesions (4). Plaque-dwelling macrophages arise from blood monocytes, and abrogating leukocyte recruitment drastically reduces atherosclerotic plaque development and complication in mice (5–12). After myocardial infarction (MI), the hematopoietic system produces excess inflammatory cells (13, 14) that accelerate plaque growth in mice (15) and enhance systemic plaque inflammation in humans (16, 17). Owing to this increase in inflammation, previously asymptomatic lesions may become unstable and trigger subsequent MI. Recurrent ischemic events have accentuated case fatality (18). If leukocyte recruitment could be interrupted, then plaque inflammation may wane, rendering arteries less prone to rupture. Patients with acute MI and a high in flammatory burden could specifically benefit from such a treatment, which potentially prevents further ischemic events.

Neutrophils and monocytes rely on endothelial cell adhesion molecules (CAMs) and interaction between chemokines and their receptors for recruitment into the arterial wall. Cell recruitment is a multistep process that involves rolling (mediated by E- and P-Selectins), firm arrest and adhesion [mediated by vascular cell adhesion molecule 1 (VCAM-1) and intercellular cell adhesion molecule 1 (ICAM-1)], and endothelial transmigration (mediated by ICAM-2) (19–22). Endothelial cells that line atherosclerotic plaques express high levels of collaborating leukocyte adhesion molecules (2, 19, 20, 22–24). Loss-of-function studies investigating single CAMs demonstrate their importance for the development of atherosclerosis (7, 25). Data obtained in mice with genetic deficiency for more than one CAM suggest that inhibiting adhesion molecule function in parallel has synergistic effects on leukocyte recruitment (8, 24). We thus reasoned that simultaneously

inhibiting five disease-associated adhesion molecules would inhibit leukocyte recruitment effectively and reduce arterial inflammation, especially during post-MI disease acceleration.

Because small interfering RNA (siRNA) inhibits gene expression by mediating mRNA cleavage in a sequence-specific manner, concurrently delivering five distinct siRNAs offers an appealing approach to reduce the translation of multiple targets with high specificity. However, combination therapies require highly efficient delivery vehicles, which have historically been limited to hepatocyte targeting (26). We recently developed a nontoxic nanoformulation that delivers siRNA to endothelial cells at very low doses (27). Here, we use these endothelial-avid nanoparticles to reduce simultaneously the expression of five endothelial CAM in *ApoE*$^{-/-}$ mice with accelerated atherosclerosis after MI. This quintuple-target drug candidate, termed siCAM^5, decreased leukocyte recruitment and plaque inflammation. Similarly, siCAM^5 treatment lowered immune cell infiltration into acutely ischemic myocardium and improved post-MI recovery in mice. Our study suggests the viability of targeting multiple genes in parallel as a therapeutic avenue for inhibiting inflammatory aspects of atherosclerotic disease progression after a myocardial ischemic insult.

RESULTS

Arterial sympathetic activity increases plaque leukocytes after MI

Accelerated leukocyte production in the spleen and bone marrow after MI increases plaque leukocyte numbers. After coronary ligation in mice, sympathetic nervous system signaling in the bone marrow contributes to this phenomenon (15). Because previous studies indicated that sympathetic tone also regulates circadian fluctuation of adhesion molecule expression in endothelial cells (28), we explored whether increased vascular wall sympathetic nervous tone may also contribute to post-MI arterial inflammation. First, we differentiated circulating from noncirculating factors by joining *ApoE*$^{-/-}$ mice in parabiosis. After 2 weeks, during which shared circulation developed, we induced MI in one parabiont only (Fig. 1A). Comparing the vasculature of the infarcted and the noninfarcted parabiont, so we reasoned, would allow us to study effects that are not related to blood-borne signals or circulating cells. Three weeks after coronary artery ligation, the infarcted and noninfarcted mice sharing circulation in parabiosis had similarly elevated blood leukocytosis when compared to steady-state parabionts without MI (Fig. 1B). However, the infarcted parabionts recruited more neutrophils and Ly6C^{high} monocytes into their aortae, consequently yielding higher plaque macrophage numbers than both their noninfarcted partners and steady-state parabionts (Fig. 1C). Plaque size was larger in the infarcted than in noninfarcted parabionts (Fig. 1D). These data indicate that circulation-independent processes contribute to acceleration of atherosclerosis after MI, as infarcted parabionts recruited more cells despite similar blood leukocyte supply.

We next investigated atherosclerotic plaque endothelial expression of CAM and chemokines after MI in single *ApoE*$^{-/-}$ mice by using flow cytometry of aortic endothelial cells (fig. S1). ICAM-1, ICAM-2, VCAM-1, E-*Sele*ctin, and P-*Sele*ctin levels are known to rise on inflamed, plaque-lining endothelial cells in mice (2, 19, 20, 22–24). Three days after MI, aortic endothelial ICAM-2, VCAM-1, and E-Selectin protein amounts increased (Fig. 2, A

and B). Endothelial expression of the CCR2 ligand *Mcp1* rose on day 3 after coronary ligation, likely also supporting increased monocyte recruitment into plaques after MI (Fig. 2C). Parabiosis experiments, similar to those examining cellular recruitment described in Fig. 1, revealed higher protein levels of ICAM-2, VCAM-1, and E-Selectin in the aortae of infarcted versus noninfarcted parabionts (Fig. 2, D and E), indicating that circulation-independent processes contributed to the rise in CAM levels after MI.

To explore the role of the sympathetic nervous system in modulating CAM expression after MI, we stained whole-mount aortic roots for tyrosine hydroxylase. This rate-limiting enzyme, located in adventitial sympathetic nervous fibers, regulates noradrenaline synthesis by catalyzing the tyrosine conversion to L-3,4-dihydroxyphenylalanine (L-dopa). Aortic tyrosine hydroxylase staining increased after MI (Fig. 3A), as did tyrosine hydroxylase mRNA in aortic roots (Fig. 3B). In $ApoE^{-/-}$ mice, aortic arch noradrenaline, a sympathetic neuro-transmitter, increased after permanent coronary ligation (Fig. 3C). Noradrenaline levels after ischemia/reperfusion injury in wild-type mice were slightly but not significantly lower than after MI (Fig. 3D). As expected, ablating the sympathetic nervous system with 6-hydroxydopamine (6-OHDA) dampened the increase in nor-adrenaline (Fig. 3C). It attenuated the increase of ICAM-2, VCAM-1, and E-Selectin on plaque endothelial cells after MI (Fig. 3E).

Next, we addressed whether aortic endothelial cells can directly sense locally released noradrenaline. Aortic endothelial cells expressed both α- and β-adrenergic receptors (Fig. 3F), suggesting that sympathetic nervous system activity enhances arterial leukocyte recruitment via increased CAM expression, possibly by local action on endothelial cells.

Plaque endothelial cells take up nanoparticle siRNA carriers

Limiting CAM expression may provide a therapeutic option to counteract leukocyte recruitment after MI. Viable siRNA sequences targeting CAM were identified by in vitro screening of in silico–predicted candidates (fig. S2A and table S1). The best duplexes were selected for scale-up and nanoparticle formulation and modified to minimize immunostimulation and off-target silencing (29). We delivered all siRNAs with a nanoparticle recently optimized for in vivo delivery to endothelial cells (27). These nanoparticles were formulated with either control siRNA targeting luciferase (termed siCtrl) or a combination of five siRNAs targeting *Icam1*, *Icam2*, *Vcam1*, *Sele*, and *Selp* (termed $siCAM^5$). Reflecting their individual in vitro siRNA potency (fig. S2B), the five siRNAs were admixed in a molar ratio of 1:0.35:1:1:1, with siRNA targeting *Icam2* being represented at 0.35 (fig. S3A). After formulation with siCtrl or $siCAM^5$, transmission electron microscopy revealed siRNA and lipid multilamellar structures with a particle diameter 45 ± 16 nm (SD) measured by dynamic light scattering (fig. S3, B and C).

To examine how effectively these particles delivered siRNA to arterial endothelial cells in $ApoE^{-/-}$ mice with atherosclerosis, we formulated fluorochrome-conjugated siRNA in nanoparticles and injected them intravenously (1.0 mg/kg siRNA). Two hours later, fluorescent signal was detected histologically in $CD31^{high}$ endothelial cells lining atherosclerotic plaques in the aortic root and arch (fig. S3D). Cy3-labeled siRNA was undetectable in deeper plaque layers (fig. S3, E and F). To quantify in vivo siRNA delivery,

we measured uptake in aortic endothelial cells, blood leukocytes, and plaque macrophages by flow cytometry. The fluorescence intensity increased more than 54-fold in $CD45^{low}$ $CD31^{high}$ $CD107a^{high}$ endothelial cells isolated from aortae (fig. S3G), indicating effective siRNA delivery to endothelial cells. In line with the histologic findings, plaque macrophages lacked siRNA (fig. S4A). In contrast, blood neutrophils and monocytes incorporated siRNA, but to a far lesser extent than endothelial cells (28- and 11-fold lower, respectively; fig. S4B).

Next, we measured five target genes' mRNA and protein levels in aortic endothelial cells in vivo. Over the course of 1 week, mice were injected twice with siCtrl (3 mg/kg) or $siCAM^5$ before $CD45^{low}$ $CD31^{high}$ $CD107a^{high}$ cells were flow-sorted from $ApoE^{-/-}$ aortae. Compared to siCtrl-treated mice, those that received $siCAM^5$ treatment had significantly decreased target gene mRNA and protein levels (Fig. 4). With RNA interference (RNAi), there was no significant reduction in circulating cells (fig. S5A), and the overall profile of circulating myeloid cells was comparable between the siCtrl and $siCAM^5$, with the exception of *Il1*β, *Tnf*α, and *Mpo* (fig. S5B). Total blood cholesterol levels were unchanged after treatment with $siCAM^5$ (fig. S6).

$siCAM^5$ treatment suppresses leukocyte recruitment to atherosclerotic plaques

To determine whether $siCAM^5$ treatment curtails leukocyte recruitment to atherosclerotic plaques in vivo, we treated $ApoE^{-/-}$ mice with $siCAM^5$ over a period of 2 weeks (three intravenous injections of 3 mg/kg cumulative siRNA dose) before adoptive intravenous transfer of 2 million green fluorescent protein–positive (GFP^+) neutrophils admixed with 2 million GFP^+ $Ly6C^{high}$ monocytes. These myeloid cells, which rely on adhesion molecules for recruitment into plaques, promote plaque growth and inflammation (1, 2). Two days after cell transfer, the number of GFP^+ $CD11b^{high}$ myeloid cells recruited into the aortae of $siCAM^5$-treated mice was 50% lower than in mice treated with siCtrl, whereas their numbers in blood were similar (Fig. 5A).

With respect to plaque character in $ApoE^{-/-}$ mice, although circulating neutrophils and $Ly6C^{high}$ monocytes did not change, their numbers decreased in the aortae by at least one-third (Fig. 5, B and C). The number of plaque macrophages also decreased (Fig. 5B). Immunohistochemical and real-time quantitative polymerase chain reaction (RT-qPCR) studies further supported reduced leukocyte recruitment by $siCAM^5$ treatment. Specifically, we observed at least 40% reduction in myeloid cells and neutrophils in aortic root sections stained for myeloid markers CD11b and Ly6G (Fig. 5D).

To explore whether parallel silencing of multiple CAMs is synergistic, we compared aortic leukocyte numbers in mice treated with $siCAM^5$ with mice treated with a single siRNA at a similar cumulative dose. We chose silencing *Vcam1* because its involvement in atherosclerosis is well documented (19). Treatment with si*Vcam1* reduced aortic neutrophil, monocyte, and macrophage numbers compared with siCtrl but was significantly less effective than $siCAM^5$ (Fig. 5E). To compare blockade of distinct steps in the recruitment cascade, we injected $ApoE^{-/-}$ mice with siRNA combinations targeting either leukocyte rolling (*Sele* and *Selp*) or adhesion and transmigration (*Icam1*, *Icam2*, and *Vcam1*) at a

similar cumulative dose. Blocking mediators of rolling reduced monocyte uptake more efficiently than targeting adhesion and transmigration (fig. S7).

Expression of myeloperoxidase (*Mpo*), a product of neutrophils and the inflammatory monocyte subset, and F4/80, a marker for macrophages, decreased in aortic plaques of siCAM^5-treated mice by at least 75% (Fig. 6A). Atherosclerotic plaques also expressed less of the proinflammatory cytokines *Tnf*α, *Il6*, *Il1*β, and *Il12* (Fig. 6A). Matrix metalloproteinases (MMPs) released by inflammatory cells promote extracellular matrix degradation in fibrous caps, support vessel remodeling, and may destabilize atherosclerotic plaques (30). *Mmp2*, *Mmp3*, and *Mmp9* mRNA levels decreased in mice treated with siCAM^5 by up to 85% (Fig. 6A). Protease activity also significantly decreased in mice treated with siCAM^5 (Fig. 6B) and, accordingly, plaque collagen increased (Fig. 6C). As a result, we observed smaller necrotic cores and thicker fibrous caps in mice treated with siCAM^5, whereas plaque size remained unaffected by this 2-week treatment (Fig. 6D).

siCAM^5 reduces inflammation after myocardial ischemia

Because we developed siCAM^5 for a clinical scenario that necessitates rapid inflammation reduction, we tested the approach in *ApoE*$^{-/-}$ mice that underwent coronary ligation, which accelerates inflammation within atheromata (15). Mice received siCAM^5 for 3 weeks (weekly injection of 3 mg/kg siRNA) after MI. MI increased the number of inflammatory leukocytes in aortic plaques (Fig. 7A and fig. S8) and augmented both lesion and necrotic core size (Fig. 7B) compared to *ApoE*$^{-/-}$ mice that had no MI, as described previously (15). Treatment with siCAM^5 limited these post-MI changes by blocking inflammatory cell recruitment (Fig. 7A) and reducing plaque size to those of control animals without MI (Fig. 7B).

Last, we investigated whether siCAM^5 affects leukocyte recruitment in acutely ischemic myocardium, an injury that relies on leukocytes for infarct healing but that may be enhanced by an overzealous immune response (1). A single dose of siCAM^5, administered 2 hours after coronary ligation, reduced Ly6C^{high} monocyte numbers by more than 50% on day 3 after MI, whereas circulating cell numbers did not change (Fig. 7C). To assess the consequences of reduced monocyte recruitment to the ischemic heart 3 weeks after MI, we performed cardiac magnetic resonance imaging (MRI) on *ApoE*$^{-/-}$ mice that received either siCtrl or siCAM^5. Treatment with siCAM^5 preserved left ventricular ejection fraction in mice after MI (siCAM^5, 33 ± 4%; siCtrl, 23 ± 4%; Fig. 7D). In summary, RNAi efficiently attenuated myeloid recruitment to the ischemic heart and consequently improved recovery after MI.

DISCUSSION

Ischemic organ injury leading to stroke and MI remains the most prevalent cause of death worldwide (31). Previous work identified soluble and nervous signals that increase innate immune cell production during acute MI (14, 15). Here, we provide evidence that acute ischemia increases systemic expression of proteins that recruit leukocytes into plaques. The stimuli that enhance endothelial CAM expression include noncirculating factors, specifically sympathetic nervous signaling. Although recruited leukocytes dominate arterial plaque

events that lead to downstream tissue hypoxia, current clinical therapy does not target these cells. Rather, beyond reperfusion therapy, standard care targets platelets, and risk factors such as hyperlipidemia and hypertension. Further inroads into preventing recurrent events and complications of acute coronary syndromes require therapeutic options that allow rapid and decisive interventions beyond standard measures. Multiple plaques in an individual can provoke such recurrence and complications, hence the desirability of a systemic rather than local intervention. Therapeutically targeting leukocyte supply offers one promising approach, because macrophages turn over rapidly in atherosclerotic plaques (4)—a process that depends on bone marrow–derived monocytes and neutrophils. Blood leukocytosis has been correlated with adverse outcome in cardiovascular patients (32, 33), and abundant preclinical data show benefits of inhibiting pathways that recruit leukocytes (6, 8, 25, 34–36).

Leukocyte accumulation is associated with increased plaque vulnerability, thrombus formation, vascular occlusion, MI, and stroke. Macrophages have particular importance because they accumulate progressively in growing lesions, become foam cells after lipid ingestion, and promote disease by producing a myriad of proinflammatory mediators. Plaque macrophages originate from monocytes recruited from the blood pool (4). Although neutrophils have a less well understood role in atherosclerosis, these cells are increasingly recognized as inflammatory mediators that accumulate in the vessel wall during atherogenesis (37). On the basis of these data, blocking chemokine/chemokine receptor interaction and adhesion molecule function emerged as a promising strategy that has relied primarily on small-molecule inhibitors or antibodies (34, 38, 39). However, redundancies in the leukocyte recruitment cascade may affect the efficiency of single-target strategies. Here, we simultaneously silenced the expression of all known endothelial CAM. Enabled by a high-efficiency delivery nanoparticle with avidity for endothelial cells, the required siRNA doses were low enough to allow combining five duplexes into one delivery nanoparticle. This poly-target therapy had profound synergistic effects and systemically neutralized the increase of leukocyte recruitment into cardiovascular organs triggered by acute ischemia.

Our study has several limitations. The exact relative contribution of each CAM to leukocyte recruitment remains uncertain, and therefore also the relative importance of each individual siRNA contained in siCAM^5. Our studies revealed that one siRNA was less powerful in dampening leukocyte recruitment as a combination of all five siRNAs. Additional studies should clarify whether all five siRNAs are essential, or whether the nanoparticle composition could be better tailored and simplified, a desirable goal from a drug development perspective. Genetically modified mice that develop atheromata, including *ApoE*$^{-/-}$ mice, display many features of atherosclerosis that are also observed in humans, like accumulation of leukocytes, necrotic core formation, smooth muscle cell migration to the fibrous cap, and fibrotic tissue accumulation (30). Our treatment lowered plaque leukocyte numbers and reduced necrotic core expansion and fibrous cap thinning, all hallmarks of human vulnerable plaque. Other features of human atherosclerosis, such as plaque rupture and subsequent thrombus formation, are rarely observed in mice. Thus, the translatability of the data to human patients requires scrutiny. Larger animals that develop plaques, including rabbits, pigs, or monkeys, should be tested next. Our previous work

demonstrated minimal toxicity of the endothelial-avid delivery nanoparticles in mice (27). The safety of these nanoparticles needs to be established in humans.

Advances in siRNA delivery, together with siRNA modification to reduce off-target effects, have led to a resurgence in efforts to clinically translate systemic RNAi (40). We hypothesize that a short-term intravenous RNAi treatment course, similar to the one tested in *ApoE*$^{-/-}$ mice with MI, could benefit a very high risk population of patients identified by either risk scores or molecular imaging. Such intervention may also benefit patients with acute ischemic events, who may have rates of recurrent events exceeding 10% within the first year despite full standard of care (16). Initiating RNAi therapy shortly after an ischemic event may have a twofold benefit. First, the treatment could decrease recruitment of neutrophils and monocytes into the ischemic brain or myocardium, thus reducing injury (41, 42). Second, silencing endothelial CAM could attenuate the acceleration of atherosclerosis observed after MI in mice (15) and patients (43). Our data support the further pursuit of these therapeutic avenues and demonstrate the utility of multigene targeting therapies to study and treat diseases that involve endothelial dysfunction. Thus, such RNAi-based multi-gene silencing may be a safe and viable treatment paradigm for endothelial dysfunction promoted by complex genetic networks.

MATERIALS AND METHODS

Study design

To study RNAi in ischemic heart disease, we performed experiments in *ApoE*$^{-/-}$ mice that were fed a high-cholesterol diet (HCD). A power analysis justified the sample size based on the variance (for instance, for plaque leukocyte numbers) that we obtained from previous experiments in *ApoE*$^{-/-}$ mice (15). We excluded outliers that were identified by a ROUT Identify Outliers test. Leukocyte numbers, plaque size, plaque protease activity, and protein/mRNA levels were investigated as predefined end points in this study. Age- and sex-matched mice were assigned randomly to the experimental groups. Studies were not performed in a blinded fashion. Sample size and number of experimental replicates are displayed in the figure captions.

Sequence identification

The set of siRNAs targeting each gene were designed using custom R and Python scripts. The rationale and method for the set of siRNA designs are as follows: the predicted efficacy for every potential 19-mer siRNA from the start of the coding region to the end of the 3′ untranslated region (UTR) was determined with a linear model derived from the direct measure of mRNA knockdown from more than 20,000 distinct siRNA designs targeting a large number of vertebrate genes. Subsets were subsequently identified with perfect or near-perfect matches between human, rodent, and cynomolgus monkey orthologs. For each strand of the siRNA, a custom Python script was used in a brute force search to measure the number and positions of mismatches between the siRNA and all potential alignments in the target species transcriptome (defined as National Center for Bio-technology Information's RefSeq collection for each species). Extra weight was given to mismatches in the seed region, defined here as positions 2 to 9 of the antisense oligonucleotide, as well as the

cleavage site of the siRNA, defined here as positions 10 and 11 of the antisense oligonucleotide. The relative weight of the mismatches was 2.8 (1.2:1 for seed mismatches, cleavage site, and other positions up to antisense position 19). Mismatches in the first position were ignored. A specificity score was calculated for each strand by summing the value of each weighted mismatch. Preference was given to siRNAs whose antisense score in human and cynomolgus monkey was ≥3.0 and predicted efficacy was ≥70% knockdown.

Synthesis and in vitro screening of siRNAs

All RNAs were modified to reduce immune stimulation and improve specificity as described previously (29, 44). To select an siRNA for a given gene, sequences targeting the 3′UTR of the gene were synthesized and tested. The siRNAs targeting *Sele*, *Selp*, *Icam1*, and *Icam2* were transfected in bEnd.3 murine endothelial cells [American Type Culture Collection (ATCC)] using Lipofectamine 2000 (Invitrogen); the siRNAs targeting *Vcam1* were tested in C2C12 cells (ATCC). In all cases, the siRNAs were dosed at 1 nM. Lead candidates were selected from this panel and tested at various doses in bEnd.3 cells to measure in vitro potency. In all cases, target gene mRNA was normalized to murine *Gapdh*; this ratio was compared to cells that were not transfected with siRNA. In all cases, mRNA analysis was performed 48 hours after transfection, and cells were passaged in Dulbecco's modified Eagle's medium supplemented with 10% fetal bovine serum. To generate consistent inflammatory gene expression in these cell lines, the bEnd.3 cells were exposed to lipopolysaccharide (LPS; 0.01 ng/μl) (LPS-EB; InvivoGen) 1 hour before transfection, and the C2C12 cells to tumor necrosis factor–α (TNFα) (InvivoGen). The best duplexes were *Sele*cted for scale-up, formulation, and subsequent nanoparticle encapsulation.

siRNA formulation into 7C1 nanoparticles

7C1 was synthesized by reacting low–molecular weight poly(ethyleneimine) (600 daltons; Sigma-Aldrich) with an epoxide-terminated C_{15} alkyl tail in 100% ethanol at 90°C for 48 hours. After synthesizing 7C1, it was purified on a silica column with increasing amounts of dichloromethane, as described previously (27). 7C1 nanoparticles were formulated by mixing the chemical compound 7C1 with $C_{14}PEG_{2000}$ (Alnylam Pharmaceuticals) in a poly(dimethylsiloxane)-based micro-fluidic device (45). More specifically, the 7C1 compound and $C_{14}PEG_{2000}$ were solubilized in 100% ethanol and loaded into a glass syringe (Hamilton). siRNAs were solubilized in 10 mM citrate buffer (pH 4.0) and loaded into another syringe. The two 7C1/$C_{14}PEG_{2000}$ ethanol phases were mixed with the RNA citrate buffer phase at a flow ratio of 1:3 using a syringe pump (Harvard Apparatus). The fluid speeds were 600 and 1800 μl/min, respectively. Particles were then dialyzed against 1× phosphate-buffered saline at 4°C for at least 3 hours and sterilized using a 0.22-μm filter.

Nanoparticle and siRNA dosing

Nanoparticle size and structure were characterized as described in Supplementary Materials and Methods. Nanoparticles were injected intravenously via a tail vein in a volume of 10 μl/g body weight. For a 1-week study, we injected particles on days 1 and 3, and for longer studies once a week thereafter. Particles contained either siRNA (3.0 mg/kg) targeting luciferase (termed siCtrl) or a combination of five siRNAs (3.0 mg/kg) encapsulated in the same particle targeting the leukocyte adhesion molecules *Icam1*, *Icam2*, *Vcam1*, *Sele*, and

Selp (siCAM^5). Nontargeting siRNAs are frequently used as controls in siRNA studies (27, 46–50). We selected an siRNA targeting luciferase because the protein is not expressed in any mice used in this study and, as a result, could be used in any experiment. Notably, the control sequence we selected was modified at the 2′ position to avoid off-target effects and has been used previously as a control in many experiments (27, 46–50).

Mice

Female C57BL/6J mice (wild type), female ubiquitous GFP mice [C57BL/6-Tg (UBC-GFP) 30Scha/J], and female apolipoprotein E–deficient mice (*ApoE*$^{-/-}$; B6.129P2-Apoetm1Unc/J) were purchased from The Jackson Laboratory. At 12 weeks of age, *ApoE*$^{-/-}$ mice were fed an HCD (21.2% fat by weight and 0.2% cholesterol; TD.88137, Harlan Teklad) for 3 to 6 weeks. All procedures were approved by the Institutional Animal Care and Use Committee (IACUC) Subcommittee on Research Animal Care, Massachusetts General Hospital (MGH), Charlestown, MA.

MI and parabiosis

MI was induced by permanent ligation of the left anterior descending coronary artery as described previously (14). *ApoE*$^{-/-}$ mice were anesthetized with isoflurane, intubated, and ventilated. All mice received buprenorphine (0.1 mg/kg, intraperitoneally) twice daily for 3 days, starting on the day of the surgery, as stipulated by the local IACUC. Sham MI surgery was carried out as described for the MI surgery, but instead of tying a knot that permanently ligated the coronary artery, the suture was not closed. Ischemia-reperfusion injury was induced as described previously (14). In brief, we ligated the left anterior descending coronary artery and released the suture after 45 min of ischemia.

Mice were joined in parabiosis as described previously (14). To induce MI, mice were anesthetized with isoflurane. All mice received buprenorphine (0.1 mg/kg, intraperitoneally) twice daily for 3 days, starting on the day of the surgery. Experiments began 14 days after induction of parabiosis so that a shared circulation was established before one parabiont was subjected to coronary artery ligation.

Statistical analysis

Statistical analyses were performed using GraphPad Prism software (GraphPad Software Inc.). Results are depicted as means ± SEM. For two-group comparisons, an unpaired two-tailed *t* test was applied to normally distributed variables (D'Agostino-Pearson omnibus normality test) and a two-tailed Mann-Whitney *U* test to non-normally distributed variables. For comparing more than two groups, an ANOVA test, followed by a Sidak's test for multiple comparisons, was applied. Because mice joined in parabiosis are considered dependent, these data were analyzed using a stepwise *t* test strategy. First, we used a two-tailed paired Wilcoxon test to compare infarcted (red; Fig. 1) with noninfarcted (blue) parabionts. A paired test was chosen for this comparison because these animals have a common blood circulation. We next performed two separate unpaired two-tailed *t* tests to compare infarcted or noninfarcted parabionts with the average of steady-state parabiosis (gray). $P < 0.05$ indicated statistical significance.

Supplementary Material

Refer to Web version on PubMed Central for supplementary material.

Acknowledgments

We thank M. Weglarz, K. Folz-Donahue, and L. Prickett-Rice from the Flow Cytometry Core Facility, MGH, Center for Regenerative Medicine and Harvard Stem Cell Institute, and M. Waring and A. Chicoine from Ragon Institute (MGH, Massachusetts Institute of Technology, and Harvard) for assistance with cell sorting; M. Sebas (MGH) for help with mouse surgery; and L. Altstein (biostatistician; MGH Biostatistics Center) for help with statistics. **Funding:** This work was funded by grants from the NIH (HL114477, HL117829, HL096576, and K99-HL121076), the MGH Research Scholar Award, and Harvard Catalyst/The Harvard Clinical and Translational Science Center (National Center for Research Resources and the National Center for Advancing Translational Sciences, NIH Award UL1 TR001102). H.B.S. and T.H. were funded by Deutsche Forschungsgemeinschaft (SA1668/2-1 and HE-6382/1-1).

REFERENCES AND NOTES

1. Swirski FK, Nahrendorf M. Leukocyte behavior in atherosclerosis, myocardial infarction, and heart failure. Science. 2013; 339:161–166. [PubMed: 23307733]
2. Ley K, Miller YI, Hedrick CC. Monocyte and macrophage dynamics during atherogenesis. Arterioscler. Thromb. Vasc. Biol. 2011; 31:1506–1516. [PubMed: 21677293]
3. Galkina E, Ley K. Vascular adhesion molecules in atherosclerosis. Arterioscler. Thromb. Vasc. Biol. 2007; 27:2292–2301. [PubMed: 17673705]
4. Robbins CS, Hilgendorf I, Weber GF, Theurl I, Iwamoto Y, Figueiredo J-L, Gorbatov R, Sukhova GK, Gerhardt LMS, Smyth D, Zavitz CCJ, Shikatani EA, Parsons M, van Rooijen N, Lin HY, Husain M, Libby P, Nahrendorf M, Weissleder R, Swirski FK. Local proliferation dominates lesional macrophage accumulation in atherosclerosis. Nat. Med. 2013; 19:1166–1172. [PubMed: 23933982]
5. Bourdillon M-C, Poston RN, Covacho C, Chignier E, Bricca G, McGregor JL. ICAM-1 deficiency reduces atherosclerotic lesions in double-knockout mice (ApoE$^{-/-}$/ICAM-1$^{-/-}$) fed a fat or a chow diet. Arterioscler. Thromb. Vasc. Biol. 2000; 20:2630–2635. [PubMed: 11116064]
6. Collins RG, Velji R, Guevara NV, Hicks MJ, Chan L, Beaudet AL. P-selectin or inter-cellular adhesion molecule (ICAM)-1 deficiency substantially protects against atherosclerosis in apolipoprotein E–deficient mice. J. Exp. Med. 2000; 191:189–194. [PubMed: 10620617]
7. Cybulsky MI, Iiyama K, Li H, Zhu S, Chen M, Iiyama M, Davis V, Gutierrez-Ramos J-C, Connelly PW, Milstone DS. A major role for VCAM-1, but not ICAM-1, in early atherosclerosis. J. Clin. Invest. 2001; 107:1255–1262. [PubMed: 11375415]
8. Dong ZM, Chapman SM, Brown AA, Frenette PS, Hynes RO, Wagner DD. The combined role of P- and E-selectins in atherosclerosis. J. Clin. Invest. 1998; 102:145–152. [PubMed: 9649568]
9. Dong ZM, Brown AA, Wagner DD. Prominent role of P-selectin in the development of advanced atherosclerosis in ApoE-deficient mice. Circulation. 2000; 101:2290–2295. [PubMed: 10811597]
10. Iiyama K, Hajra L, Iiyama M, Li H, DiChiara M, Medoff BD, Cybulsky MI. Patterns of vascular cell adhesion molecule-1 and intercellular adhesion molecule-1 expression in rabbit and mouse atherosclerotic lesions and at sites predisposed to lesion formation. Circ. Res. 1999; 85:199–207. [PubMed: 10417402]
11. Johnson RC, Chapman SM, Dong ZM, Ordovas JM, Mayadas TN, Herz J, Hynes RO, Schaefer EJ, Wagner DD. Absence of P-selectin delays fatty streak formation in mice. J. Clin. Invest. 1997; 99:1037–1043. [PubMed: 9062362]
12. Nakashima Y, Raines EW, Plump AS, Breslow JL, Ross R. Upregulation of VCAM-1 and ICAM-1 at atherosclerosis-prone sites on the endothelium in the ApoE-deficient mouse. Arterioscler. Thromb. Vasc. Biol. 1998; 18:842–851. [PubMed: 9598845]
13. Dutta P, Sager HB, Stengel KR, Naxerova K, Courties G, Saez B, Silberstein L, Heidt T, Sebas M, Sun Y, Wojtkiewicz G, Feruglio PF, King K, Baker JN, van der Laan AM, Borodovsky A, Fitzgerald K, Hulsmans M, Hoyer F, Iwamoto Y, Vinegoni C, Brown D, Di Carli M, Libby P,

Hiebert SW, Scadden DT, Swirski FK, Weissleder R, Nahrendorf M. Myocardial infarction activates CCR2^{+} hematopoietic stem and progenitor cells. Cell Stem Cell. 2015; 16:477–487. [PubMed: 25957903]

14. Sager HB, Heidt T, Hulsmans M, Dutta P, Courties G, Sebas M, Wojtkiewicz GR, Tricot B, Iwamoto Y, Sun Y, Weissleder R, Libby P, Swirski FK, Nahrendorf M. Targeting interleukin-1β reduces leukocyte production after acute myocardial infarction. Circulation. 2015; 132:1880–1890. [PubMed: 26358260]
15. Dutta P, Courties G, Wei Y, Leuschner F, Gorbatov R, Robbins CS, Iwamoto Y, Thompson B, Carlson AL, Heidt T, Majmudar MD, Lasitschka F, Etzrodt M, Waterman P, Waring MT, Chicoine AT, van der Laan AM, Niessen HWM, Piek JJ, Rubin BB, Butany J, Stone JR, Katus HA, Murphy SA, Morrow DA, Sabatine MS, Vinegoni C, Moskowitz MA, Pittet MJ, Libby P, Lin CP, Swirski FK, Weissleder R, Nahrendorf M. Myocardial infarction accelerates atherosclerosis. Nature. 2012; 487:325–329. [PubMed: 22763456]
16. Goldstein JA, Demetriou D, Grines CL, Pica M, Shoukfeh M, O'Neill WW. Multiple complex coronary plaques in patients with acute myocardial infarction. N. Engl. J. Med. 2000; 343:915–922. [PubMed: 11006367]
17. Wald DS, Morris JK, Wald NJ, Chase AJ, Edwards RJ, Hughes LO, Berry C, Oldroyd KG, the PRAMI Investigators. Randomized trial of preventive angioplasty in myocardial infarction. N. Engl. J. Med. 2013; 369:1115–1123. [PubMed: 23991625]
18. Mega JL, Braunwald E, Wiviott SD, Bassand J-P, Bhatt DL, Bode C, Burton P, Cohen M, Cook-Bruns N, Fox KAA, Goto S, Murphy SA, Plotnikov AN, Schneider D, Sun X, Verheugt FW, Gibson CM, the ATLAS ACS 2–TIMI 51 Investigators. Rivaroxaban in patients with a recent acute coronary syndrome. N. Engl. J. Med. 2012; 366:9–19. [PubMed: 22077192]
19. Ley K, Laudanna C, Cybulsky MI, Nourshargh S. Getting to the site of inflammation: The leukocyte adhesion cascade updated. Nat. Rev. Immunol. 2007; 7:678–689. [PubMed: 17717539]
20. Moore KJ, Sheedy FJ, Fisher EA. Macrophages in atherosclerosis: A dynamic balance. Nat. Rev. Immunol. 2013; 13:709–721. [PubMed: 23995626]
21. Rao RM, Yang L, Garcia-Cardena G, Luscinskas FW. Endothelial-dependent mechanisms of leukocyte recruitment to the vascular wall. Circ. Res. 2007; 101:234–247. [PubMed: 17673684]
22. Shi C, Pamer EG. Monocyte recruitment during infection and inflammation. Nat. Rev. Immunol. 2011; 11:762–774. [PubMed: 21984070]
23. Mestas J, Ley K. Monocyte-endothelial cell interactions in the development of atherosclerosis. Trends Cardiovasc. Med. 2008; 18:228–232. [PubMed: 19185814]
24. Ley K. The role of selectins in inflammation and disease. Trends Mol. Med. 2003; 9:263–268. [PubMed: 12829015]
25. Nageh MF, Sandberg ET, Marotti KR, Lin AH, Melchior EP, Bullard DC, Beaudet AL. Deficiency of inflammatory cell adhesion molecules protects against atherosclerosis in mice. Arterioscler. Thromb. Vasc. Biol. 1997; 17:1517–1520. [PubMed: 9301629]
26. Haussecker D, Kay MA. RNA interference. Drugging RNAi. Science. 2015; 347:1069–1070. [PubMed: 25745148]
27. Dahlman JE, Barnes C, Khan O, Thiriot A, Jhunjunwala S, Shaw TE, Xing Y, Sager HB, Sahay G, Speciner L, Bader A, Bogorad RL, Yin H, Racie T, Dong Y, Jiang S, Seedorf D, Dave A, Sandu KS, Webber MJ, Novobrantseva T, Ruda VM, Lytton-Jean AKR, Levins CG, Kalish B, Mudge DK, Perez M, Abezgauz L, Dutta P, Smith L, Charisse K, Kieran MW, Fitzgerald K, Nahrendorf M, Danino D, Tuder RM, von Andrian UH, Akinc A, Panigrahy D, Schroeder A, Kotelianski V, Langer R, Anderson DG. In vivo endothelial siRNA delivery using polymeric nanoparticles with low molecular weight. Nat. Nanotechnol. 2014; 9:648–655. [PubMed: 24813696]
28. Scheiermann C, Kunisaki Y, Lucas D, Chow A, Jang J-E, Zhang D, Hashimoto D, Merad M, Frenette PS. Adrenergic nerves govern circadian leukocyte recruitment to tissues. Immunity. 2012; 37:290–301. [PubMed: 22863835]
29. Whitehead KA, Dahlman JE, Langer RS, Anderson DG. Silencing or stimulation? siRNA delivery and the immune system. Annu. Rev. Chem. Biomol. Eng. 2011; 2:77–96. [PubMed: 22432611]

30. Silvestre-Roig C, de Winther MP, Weber C, Daemen MJ, Lutgens E, Soehnlein O. Atherosclerotic plaque destabilization: Mechanisms, models, and therapeutic strategies. Circ. Res. 2014; 114:214–226. [PubMed: 24385514]
31. World Health Organization Report. Jul. 2013 www.who.int/mediacentre/factsheets/fs310/en/
32. Madjid M, Awan I, Willerson JT, Casscells SW. Leukocyte count and coronary heart disease: Implications for risk assessment. J. Am. Coll. Cardiol. 2004; 44:1945–1956. [PubMed: 15542275]
33. Coller BS. Leukocytosis and ischemic vascular disease morbidity and mortality: Is it time to intervene? Arterioscler. Thromb. Vasc. Biol. 2005; 25:658–670. [PubMed: 15662026]
34. Huo Y, Hafezi-Moghadam A, Ley K. Role of vascular cell adhesion molecule-1 and fibronectin connecting segment-1 in monocyte rolling and adhesion on early atherosclerotic lesions. Circ. Res. 2000; 87:153–159. [PubMed: 10904000]
35. Huang M-T, Larbi KY, Scheiermann C, Woodfin A, Gerwin N, Haskard DO, Nourshargh S. ICAM-2 mediates neutrophil transmigration in vivo: Evidence for stimulus specificity and a role in PECAM-1–independent transmigration. Blood. 2006; 107:4721–4727. [PubMed: 16469869]
36. Elices MJ, Osborn L, Takada Y, Crouse C, Luhowskyj S, Hemler ME, Lobb RR. VCAM-1 on activated endothelium interacts with the leukocyte integrin VLA-4 At a site distinct from the VLA-4/fibronectin binding site. Cell. 1990; 60:577–584. [PubMed: 1689216]
37. Soehnlein O. Multiple roles for neutrophils in atherosclerosis. Circ. Res. 2012; 110:875–888. [PubMed: 22427325]
38. Kaneider NC, Leger AJ, Kuliopulos A. Therapeutic targeting of molecules involved in leukocyte–endothelial cell interactions. FEBS J. 2006; 273:4416–4424. [PubMed: 16956369]
39. Ulbrich H, Eriksson EE, Lindbom L. Leukocyte and endothelial cell adhesion molecules as targets for therapeutic interventions in inflammatory disease. Trends Pharmacol. Sci. 2003; 24:640–647. [PubMed: 14654305]
40. Crunkhorn S. Trial watch: Pioneering RNAi therapy shows antitumour activity in humans. Nat. Rev. Drug. Discov. 2013; 12:178. [PubMed: 23449295]
41. Leuschner F, Dutta P, Gorbatov R, Novobrantseva TI, Donahoe JS, Courties G, Lee KM, Kim JI, Markmann JF, Marinelli B, Panizzi P, Lee WW, Iwamoto Y, Milstein S, Epstein-Barash H, Cantley W, Wong J, Cortez-Retamozo V, Newton A, Love K, Libby P, Pittet MJ, Swirski FK, Koteliansky V, Langer R, Weissleder R, Anderson DG, Nahrendorf M. Therapeutic siRNA silencing in inflammatory monocytes in mice. Nat. Biotechnol. 2011; 29:1005–1010. [PubMed: 21983520]
42. Ishikawa M, Zhang JH, Nanda A, Granger DN. Inflammatory responses to ischemia and reperfusion in the cerebral microcirculation. Front. Biosci. 2004; 9:1339–1347. [PubMed: 14977549]
43. Kotani, J.-i.; Mintz, GS.; Castagna, MT.; Pinnow, E.; Berzingi, CO.; Bui, AB.; Pichard, AD.; Satler, LF.; Suddath, WO.; Waksman, R.; Laird, JR., Jr.; Kent, KM.; Weissman, NJ. Intravascular ultrasound analysis of infarct-related and non–infarct-related arteries in patients who presented with an acute myocardial infarction. Circulation. 2003; 107:2889–2893. [PubMed: 12782565]
44. Deleavey GF, Damha MJ. Designing chemically modified oligonucleotides for targeted gene silencing. Chem. Biol. 2012; 19:937–954. [PubMed: 22921062]
45. Chen D, Love KT, Chen Y, Eltoukhy AA, Kastrup C, Sahay G, Jeon A, Dong Y, Whitehead KA, Anderson DG. Rapid discovery of potent siRNA-containing lipid nanoparticles enabled by controlled microfluidic formulation. J. Am. Chem. Soc. 2012; 134:6948–6951. [PubMed: 22475086]
46. Love KT, Mahon KP, Levins CG, Whitehead KA, Querbes W, Dorkin JR, Qin J, Cantley W, Qin LL, Racie T, Frank-Kamenetsky M, Yip KN, Alvarez R, Sah DWY, de Fougerolles A, Fitzgerald K, Koteliansky V, Akinc A, Langer R, Anderson DG. Lipid-like materials for low-dose, in vivo gene silencing. Proc. Natl. Acad. Sci. U.S.A. 2010; 107:1864–1869. [PubMed: 20080679]
47. Semple SC, Akinc A, Chen J, Sandhu AP, Mui BL, Cho CK, Sah DWY, Stebbing D, Crosley EJ, Yaworski E, Hafez IM, Dorkin JR, Qin J, Lam K, Rajeev KG, Wong KF, Jeffs LB, Nechev L, Eisenhardt ML, Jayaraman M, Kazem M, Maier MA, Srinivasulu M, Weinstein MJ, Chen Q, Alvarez R, Barros SA, De S, Klimuk SK, Borland T, Kosovrasti V, Cantley WL, Tam YK, Manoharan M, Ciufolini MA, Tracy MA, de Fougerolles A, MacLachlan I, Cullis PR, Madden

TD, Hope MJ. Rational design of cationic lipids for siRNA delivery. Nat. Biotechnol. 2010; 28:172–176. [PubMed: 20081866]

48. Fehring V, Schaeper U, Ahrens K, Santel A, Keil O, Eisermann M, Giese K, Kaufmann J. Delivery of therapeutic siRNA to the lung endothelium via novel lipoplex formulation DACC. Mol. Ther. 2014; 22:811–820. [PubMed: 24390281]
49. Dong Y, Love KT, Dorkin JR, Sirirungruang S, Zhang Y, Chen D, Bogorad RL, Yin H, Chen Y, Vegas AJ, Alabi CA, Sahay G, Olejnik KT, Wang W, Schroeder A, Lytton-Jean AKR, Siegwart DJ, Akinc A, Barnes C, Barros SA, Carioto M, Fitzgerald K, Hettinger J, Kumar V, Novobrantseva TI, Qin J, Querbes W, Koteliansky V, Langer R, Anderson DG. Lipopeptide nanoparticles for potent and selective siRNA delivery in rodents and nonhuman primates. Proc. Natl. Acad. Sci. U.S.A. 2014; 111:3955–3960. [PubMed: 24516150]
50. Aleku M, Schulz P, Keil O, Santel A, Schaeper U, Dieckhoff B, Janke O, Endruschat J, Durieux B, Röder N, Löffler K, Lange C, Fechtner M, Möpert K, Fisch G, Dames S, Arnold W, Jochims K, Giese K, Wiedenmann B, Scholz A, Kaufmann J. Atu027, a liposomal small interfering RNA formulation targeting protein kinase N3, inhibits cancer progression. Cancer Res. 2008; 68:9788–9798. [PubMed: 19047158]

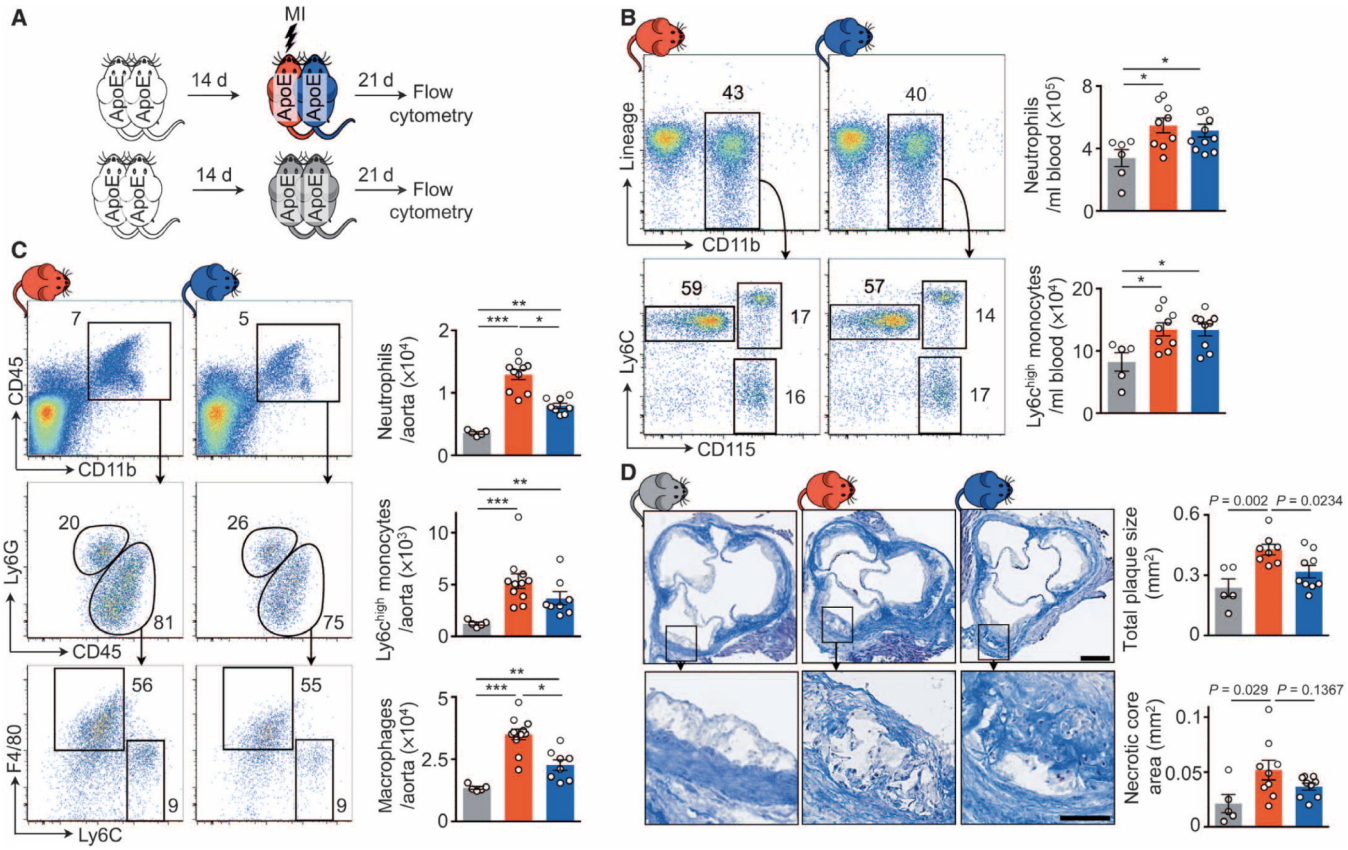

Fig. 1. Noncirculating factors contribute to expansion of inflammatory plaque leukocytes and acceleration of atherosclerosis

(**A**) Experimental setup. *ApoE*$^{-/-}$ mice were joined in parabiosis, and one parabiont was infarcted 2 weeks thereafter. Three weeks later, leukocytes were evaluated by flow cytometry. (**B** and **C**) Flow cytometric gating and quantification of blood (B) and aortic (C) leukocytes. Data are means ± SEM (n = 5 to 11 per group from two independent experiments). *P < 0.05, **P < 0.01, ***P < 0.001, two-tailed paired Wilcoxon test for comparison between connected parabionts; two-tailed unpaired Mann-Whitney U for comparison to steady-state parabiosis. (**D**) Masson staining of aortic roots. Data are means ± SEM quantifying total plaque size and necrotic core area per section (n = 5 to 9 per group from two independent experiments). Scale bars, 250 μm (top) and 100 μm (bottom).

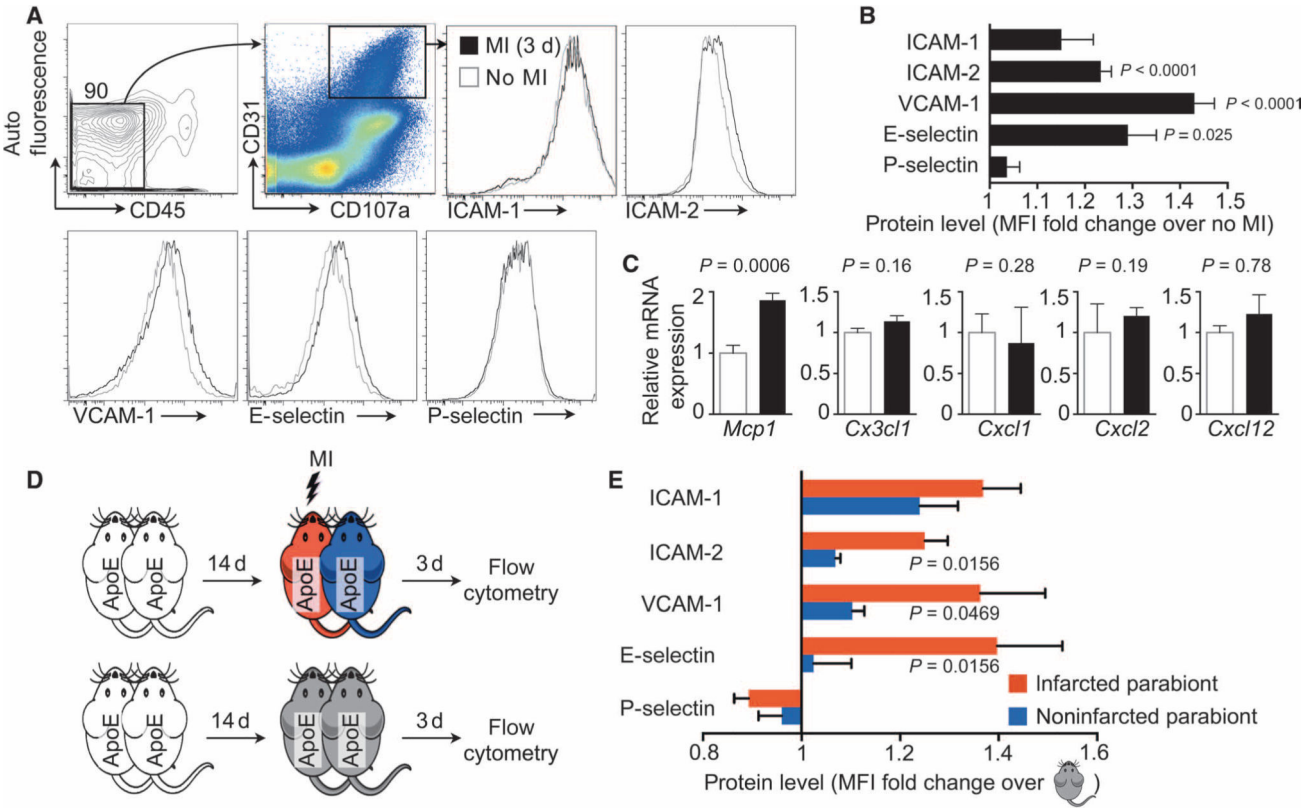

Fig. 2. Noncirculating signals contribute to expansion of plaque leukocyte recruitment after MI

(**A**) Gating strategy and histograms of leukocyte adhesion molecules on aortic endothelial cells from *ApoE*$^{-/-}$ mice 3 days after MI or no MI controls. (**B**) Mean fluorescence intensity (MFI) of adhesion molecules expressed by aortic endothelial cells from animals in (A). Data are means ± SEM (*n* = 11 to 13 per group from two independent experiments). *P* values versus no MI are determined by Mann-Whitney *U* test. (**C**) Chemokine mRNA in aortic roots from animals in (A). Data are means ± SEM (*n* = 7 to 8 per group from two independent experiments). *P* values are determined by Mann-Whitney *U* test. (**D**) Experimental setup. *ApoE*$^{-/-}$ mice were joined in parabiosis, andone parabiontwas infarcted 2 weeks thereafter. Three dayslater, CAM levels on aortic endothelial cells were evaluated by flow cytometry. (**E**) MFI on aortic endothelial cells from animals in (D) was evaluated by flow cytometry. Data are means normalized to steady-state parabiosis ± SEM (*n* = 7 per group from two independent experiments). *P* values compare respective infarcted to noninfarcted parabionts and are determined by two-tailed paired Wilcoxon test.

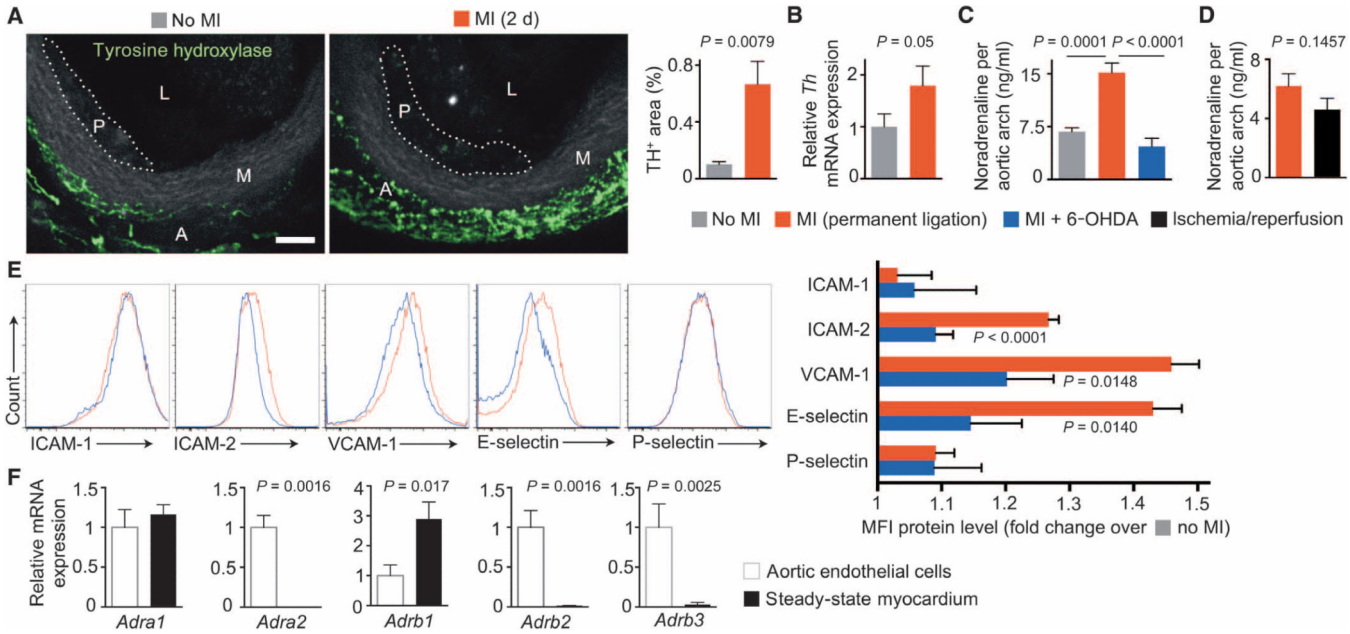

Fig. 3. Aortic sympathetic tone regulates leukocyte adhesion molecule expression after MI

These experiments examine the vascular innervation after coronary ligation. (**A**) Tyrosine hydroxylase (TH) staining of aortic roots in steady-state and infarcted atherosclerotic mice. L, lumen; M, media; A, adventitia; P, atherosclerotic plaque. Scale bar, 70 μm. TH^+ area per high-power field was quantified from fluorescent images as means ± SEM ($n = 5$ $ApoE^{-/-}$ mice per group). *P* value is determined by Mann-Whitney *U* test. (**B**) *Th* mRNA levels in aortic roots. Data are means ± SEM ($n = 7$ $ApoE^{-/-}$ mice per group from two independent experiments, normalized to controls without MI). *P* value is determined by Mann-Whitney *U* test. (**C**) Aortic arch noradrenaline content. Data are means ± SEM ($n = 4$ to 5 $ApoE^{-/-}$ mice per group). *P* values are determined by one-way analysis of variance (ANOVA). (**D**) Aortic arch noradrenaline content in permanent ligation versus 45 min of ischemia followed by reperfusion. Data are means ± SEM ($n = 8$ to 10 wild-type mice per group from two independent experiments). *P* value is determined by Mann-Whitney *U* test. (**E**) CAM expression by aortic endothelial cells in post-MI atherosclerosis (3 days after MI; red) and after MI + 6-OHDA (blue). The bar graph shows MFI on aortic endothelial cells by flow cytometry ($n = 7$ to 8 $ApoE^{-/-}$ mice per group from two independent experiments), normalized to no MI controls. *P* values are determined by one-way ANOVA. (**F**) Adrenoceptor α_{1-2} and β_{1-3} mRNA levels (*Adra* and *Adrb*) in sorted murine aortic endothelial cells. Data are means ± SEM ($n = 8$ $ApoE^{-/-}$ mice and 5 B6 mice as steady-state myocardium). *P* values are determined by Mann-Whitney *U* test.

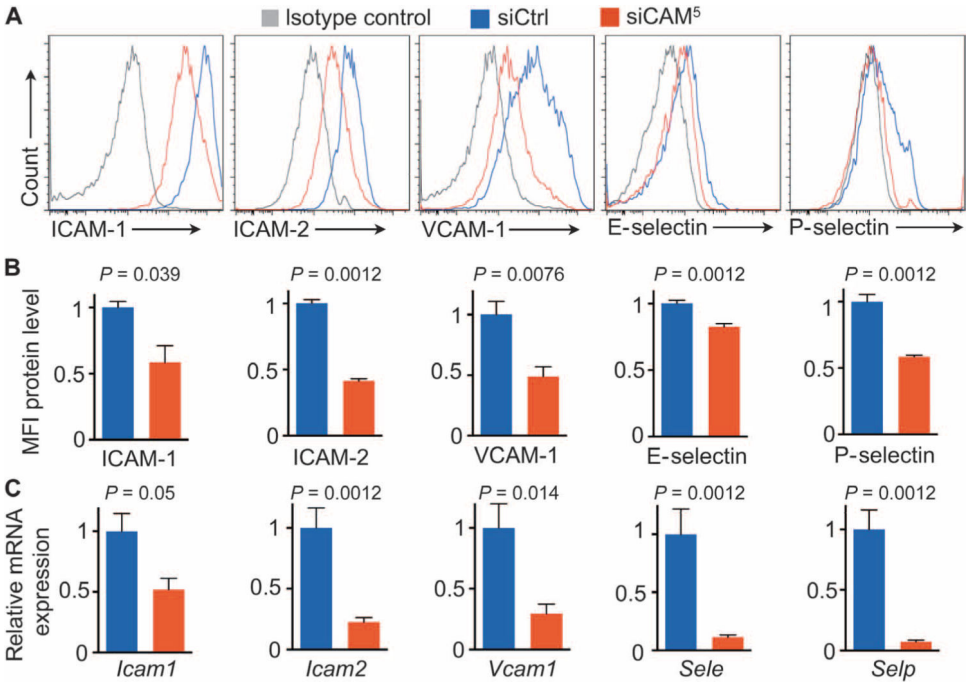

Fig. 4. siCAM^5 results in endothelial CAM knockdown

ApoE$^{-/-}$ mice were injected with either siCAM^5 or siCtrl for 1 week. (**A**) Histograms showing target proteins in murine aortic endothelial cells after RNAi. (**B**) siCAM^5 knockdown on protein level measured by flow cytometric MFI in aortic endothelial cells. Data are normalized to siCtrl. (**C**) mRNA levels after 1 week of treatment with either siCAM^5 or siCtrl. RT-qPCR data are normalized to siCtrl. Data in (B) and (C) are means ± SEM (n = 6 to 7 *ApoE*$^{-/-}$ mice per group). P values are determined by Mann-Whitney U test.

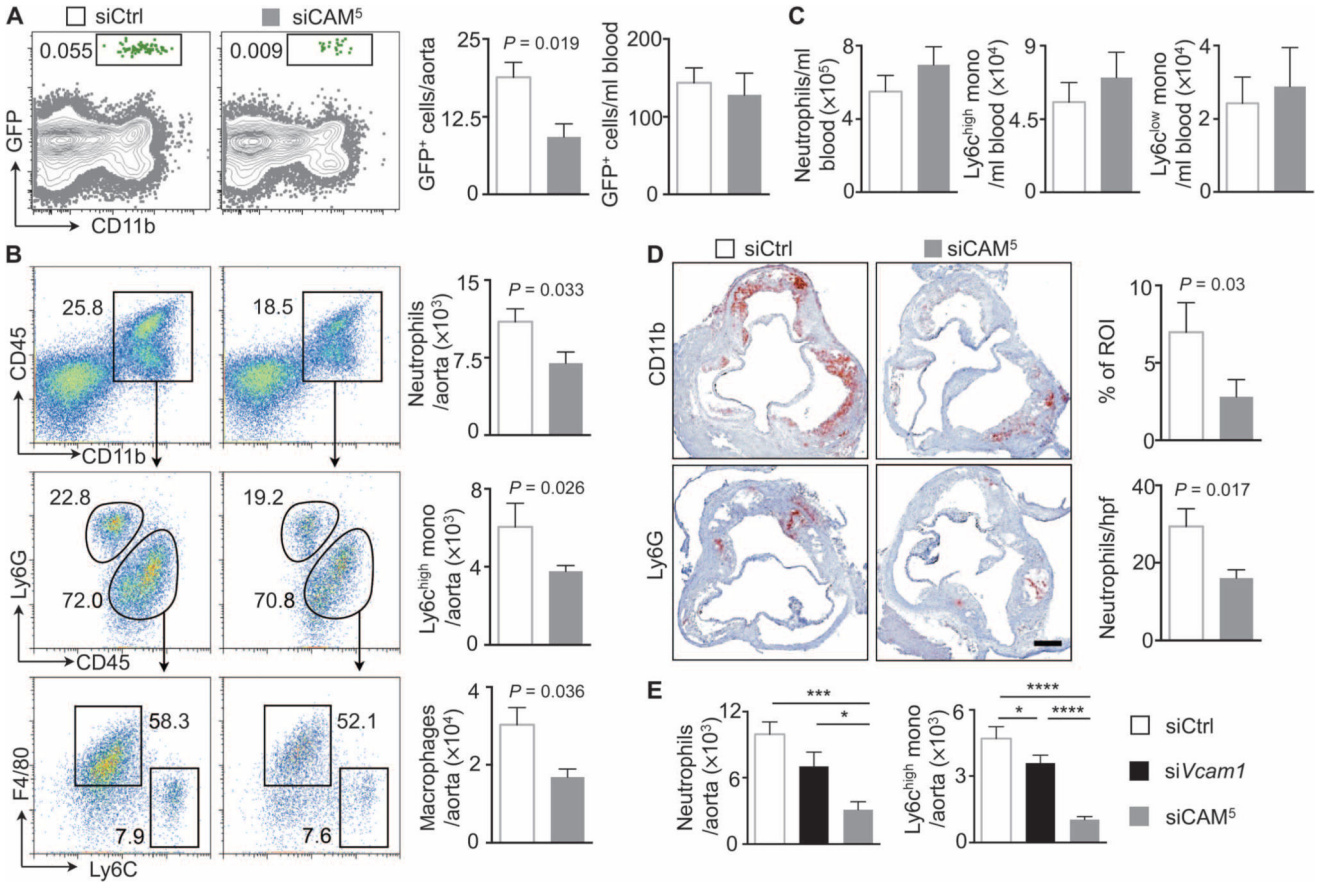

Fig. 5. siCAM^5 reduces leukocyte recruitment into plaque

ApoE$^{-/-}$ mice were injected with either siCAM^5 or siCtrl for 2 weeks. (**A**) Gating and quantification of GFP^{high} myeloid cells in plaques and quantification of GFP^{high} myeloid cells in blood after adoptive transfer of 2 × 10^6 GFP^{high} Ly6C^{high} monocytes and 2 × 10^6 GFP^{high} neutrophils. Data are means ± SEM (n = 6 to 7 *ApoE*$^{-/-}$ mice per group from two independent experiments. (**B** and **C**) Gating and quantification of neutrophils, Ly6C^{high} monocytes, and macrophages in atherosclerotic aortae (B) and in the blood (C). Data are means ± SEM (n = 6 to 10 *ApoE*$^{-/-}$ mice per group from three independent experiments). (**D**) Immunohistochemical staining of aortic roots for myeloid cells (CD11b) and neutrophils (Ly6G). Bar graphs show percentage of positive area per region of interest (ROI) or number of cells per high-power field (hpf). Scale bar, 250 μm. Data are means ± SEM (n = 5 to 6 *ApoE*$^{-/-}$ mice per group). P values in (A), (B), and (D) are determined by Mann-Whitney U test. (**E**) Quantification of neutrophils and Ly6C^{high} monocytes in athero-sclerotic aortae after treatment with siCtrl, si *Vcam1*, or siCAM^5. Data are means ± SEM (n = 7 to 8 *ApoE*$^{-/-}$ mice per group from two independent experiments). *P < 0.05, ***P < 0.001, ****P < 0.0001, one-way ANOVA.

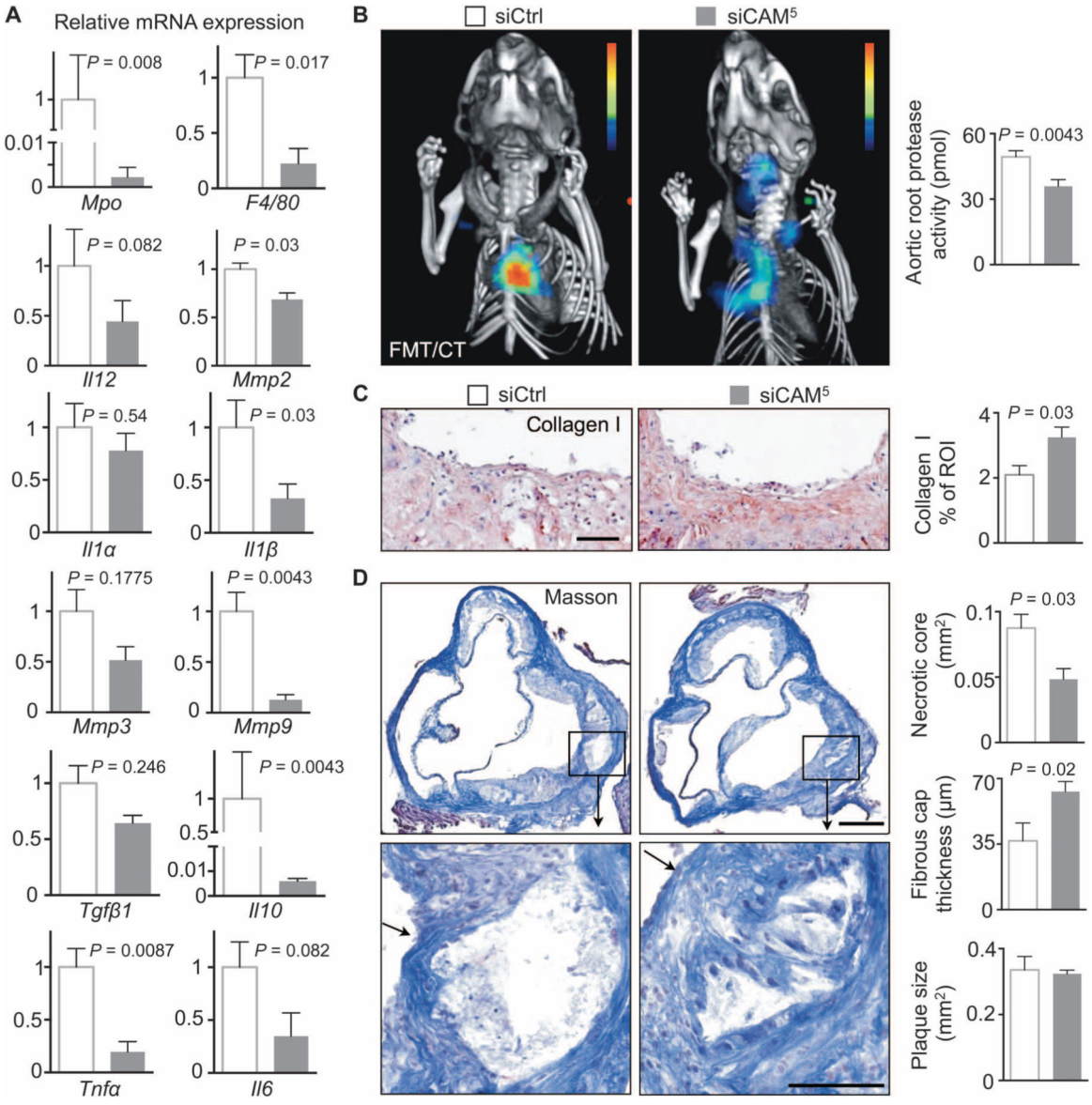

Fig. 6. siCAM^5 reduces inflammation and progression of athero-sclerotic plaque phenotype

ApoE$^{-/-}$ mice were injected with either siCAM^5 or siCtrl for 2 weeks. (**A**) mRNA levels in aortic arches; values normalized to *Gapdh* with the siCtrl group set to 1. (**B**) Aortic root protease activity by fluorescence molecular tomography (FMT)/computed tomography (CT). (**C**) Immunohistochemical evaluation of aortic roots for collagen-1 after 3 weeks of siCtrl (3 mg/kg) or siCAM5 (3 mg/kg). Bar graphs show percentage of positive staining per ROI. Scale bar, 100 μm. (**D**) Masson staining of aortic roots. Bar graphs show fibrous cap thickness, necrotic core area, and total plaque size per section. Scale bars, 250 μm (low magnification) and 100 μm (high magnification). The arrows point at a fibrous cap. In (A) to (D), data are means ± SEM (n = 5 to 6 *ApoE*$^{-/-}$ mice per group). P values are determined by Mann-Whitney U test.

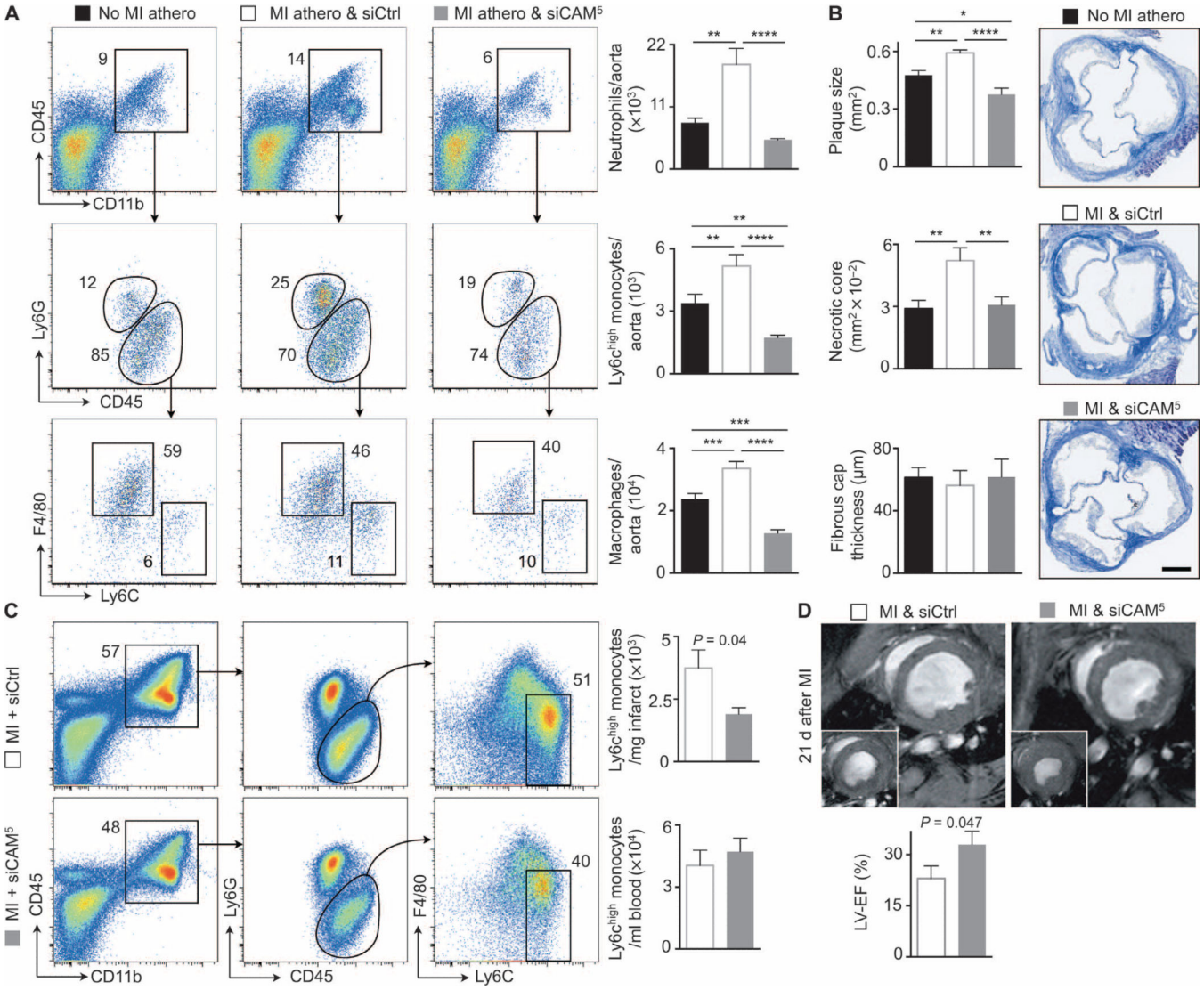

Fig. 7. siCAM^5 reduces inflammation of infarcted myocardium and improves functional recovery after ischemia

The baseline cohort of *ApoE*$^{-/-}$ mice (No MI athero) received no MI and no therapy. Cohorts of *ApoE*$^{-/-}$ mice after coronary ligation received either siCtrl (MI athero & siCtrl) or siCAM^5 (MI athero & siCAM^5) for 3 weeks. Treatment started 2 hours after MI. All cohorts are age-matched and received a similar atherogenic diet. (**A**) Gating and quantification of neutrophils, Ly6C^{high} monocytes, and macrophages in atherosclerotic aortae. Data are means ± SEM ($n = 8$ *ApoE*$^{-/-}$ mice per group from two independent experiments). *P* values are determined by one-way ANOVA. (**B**) Masson staining of aortic roots. Bar graphs show plaque size, fibrous cap thickness, and necrotic core area. Data are means ± SEM ($n = 5$ *ApoE*$^{-/-}$ mice per group). *$P < 0.05$, **$P < 0.01$, ***$P < 0.001$, ****$P < 0.0001$, one-way ANOVA. (**C**) Wild-type mice received one injection of either siCAM^5 or siCtrl 2 hours after coronary ligation. Flow cytometric gating and quantification of inflammatory monocytes in infarct and blood 3 days after MI. Data are means ± SEM ($n = 6$ mice per group). *P* values are determined by Mann-Whitney *U* test. (**D**) *ApoE*$^{-/-}$ mice

received either siCAM[5] or siCtrl for 3 weeks after coronary ligation, starting 2 hours after MI. Left ventricular ejection fraction (LV-EF) was assessed by cardiac MRI 21 days later. Data are means ± SEM (n = 5 to 6 $ApoE^{-/-}$ mice per group). P values are determined by Mann-Whitney U test.